frontiers | Frontiers in Chemistry

ORIGINAL RESEARCH
published: 07 April 2022
doi: 10.3389/fchem.2022.887439

# Molecular Rubies in Photoredox Catalysis

*Steven Sittel, Robert Naumann* and Katja Heinze**

*Department of Chemistry, Johannes Gutenberg University, Mainz, Germany*

The molecular ruby **[Cr(tpe)$_2$]$^{3+}$** and the tris(bipyridine) chromium(III) complex **[Cr(dmcbpy)$_3$]$^{3+}$** as well as the tris(bipyrazine)ruthenium(II) complex **[Ru(bpz)$_3$]$^{2+}$** were employed in the visible light-induced radical cation [4+2] cycloaddition (tpe = 1,1,1-tris(pyrid-2-yl)ethane, dmcbpy = 4,4′-dimethoxycarbonyl-2,2′-bipyridine, bpz = 2,2′-bipyrazine), while **[Cr(ddpd)$_2$]$^{3+}$** serves as a control system (ddpd = *N*,*N*′-dimethyl-*N*,*N*′-dipyridin-2-ylpyridine-2,6-diamine). Along with an updated mechanistic proposal for the Cr$^{III}$ driven catalytic cycle based on redox chemistry, Stern-Volmer analyses, UV/Vis/NIR spectroscopic and nanosecond laser flash photolysis studies, we demonstrate that the very weakly absorbing photocatalyst **[Cr(tpe)$_2$]$^{3+}$** outcompetes **[Cr(dmcbpy)$_3$]$^{3+}$** and even **[Ru(bpz)$_3$]$^{2+}$** in particular at low catalyst loadings, which appears contradictory at first sight. The high photostability, the reversible redoxchemistry and the very long excited state lifetime account for the exceptional performance and even reusability of **[Cr(tpe)$_2$]$^{3+}$** in this photoredox catalytic system.

**Keywords: chromium, radical cation, Diels-Alder reaction, [4+2] cycloaddition, photoredox catalysis, singlet oxygen**

OPEN ACCESS

***Edited by:***
*Michael Karnahl,*
*Technische Universitat Braunschweig, Germany*

***Reviewed by:***
*Oliver Wenger,*
*University of Basel, Switzerland*
*Matthias Schwalbe,*
*Humboldt University of Berlin, Germany*
*Martin Schulz,*
*Friedrich Schiller University Jena, Germany*

****Correspondence:***
*Robert Naumann*
*rnaumann@uni-mainz.de*
*Katja Heinze*
*katja.heinze@uni-mainz.de*

***Specialty section:***
*This article was submitted to Physical Chemistry and Chemical Physics, a section of the journal Frontiers in Chemistry*

***Received:*** *01 March 2022*
***Accepted:*** *17 March 2022*
***Published:*** *07 April 2022*

***Citation:***
*Sittel S, Naumann R and Heinze K (2022) Molecular Rubies in Photoredox Catalysis. Front. Chem. 10:887439. doi: 10.3389/fchem.2022.887439*

## INTRODUCTION

Complexes with long-lived luminescent metal-to-ligand charge transfer (MLCT) excited states, namely Ru$^{II}$, Ir$^{III}$, Os$^{II}$, or Re$^{I}$ complexes with polypyridine ligands, are the workhorses of many photoredox catalytic cycles, luminescent devices, sensing applications and solar energy conversion processes (Twilton, et al., 2017; Yoon, et al., 2010; Magnuson, et al., 2009; Costa, et al., 2012; Baldo, et al., 2020 Hagfeld, et al., 2010; Heinemann et al., 2017; Mari, et al., 2015; Li, et al., 2018; Yam, et al., 2020). A huge interest exists in replacing the precious metal ions by cheaper, Earth-abundant metal ions such as chromium, iron and copper and considerable progress has been achieved in the last years (Wenger, 2018; Hockin, et al., 2019; Förster and Heinze, 2020; Büldt and Wenger, 2017; Otto, et al., 2018a; Scattergood, 2020; Lindh, et al., 2020; Wenger, 2021; Hossain, et al., 2019). Reductively initiated processes were successfully employed in several instances, e.g. using Mn$^{I}$, Fe$^{II}$ and Cu$^{I}$ photocatalysts (Herr, et al., 2021; Leis, et al., 2022; Hossain, et al., 2019). Oxidative processes photoinduced by first row transition metal complexes are comparably scarce and have been reported with iron(III) and cobalt(III) (Aydogan, et al., 2021; Pal, et al., 2018) and in particular with chromium(III) photocatalysts (Stevenson, et al., 2015; Higgins, et al., 2016). Oxidatively induced photocatalytic processes, e.g. radical cation [4+2] cycloadditions, have been described by Yoon and coworkers using photooxidizing ruthenium(II) photocatalysts (Lin, et al., 2011; Farney, et al., 2019) and by Shores and others using highly photooxidizing Cr$^{III}$ complexes with 2,2′-bipyridine or 9,10-phenanthroline ligands as photocatalysts **PC$^{3+}$** (**Scheme 1A**) (Stevenson, et al., 2015; Higgins, et al., 2016; Stevenson, et al., 2017; Higgins, et al., 2018). For example, the highly oxidizing complex **[Cr(dmcbpy)$_3$]$^{3+}$** (1 mol%, $CH_3NO_2$, 300–419 nm light, 24–48 h, dmcbpy = 4,4′-

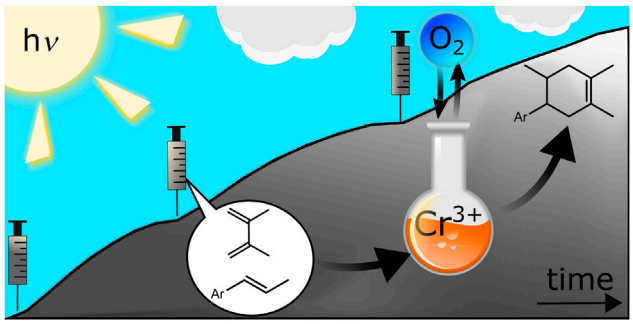


**GRAPHICAL ABSTRACT |** The molecular ruby **[Cr(tpe)$_2$]$^{3+}$** catalyzes the visible light-induced radical cation [4+2] cycloaddition with unprecedented photostability and recyclability. Detailed mechanistic studies reveal that reductive quenching of **[Cr(tpe)$_2$]$^{3+}$** is fast while the first C-C formation is the slowest step and triplet oxygen is required to rapidly regenerate **[Cr(tpe)$_2$]$^{3+}$** and prevent detrimental back-electron transfer.

dimethoxycarbonyl-2,2′-bipyridine) catalyzes the Diels-Alder reaction of various dienes such as 2,3-dimethyl-1,3-butadiene (**DMB**) with styrenes such as *trans*-anethole (***t*An**) to the Diels-Alder product **DAP** (**Scheme 1A**) (Stevenson, et al., 2015) $TiO_2/LiClO_4$ also catalyzed this reaction using UV light (365 nm, Nakayama, et al., 2019). Radical cations ***t*An**$^{\bullet+}$ and **DAP**$^{\bullet+}$ are the proposed key intermediates in this radical cation [4+2] cycloaddition, but they were never observed in this context (**Scheme 1A**). The ***t*An** radical cation ***t*An**$^{\bullet+}$ had been independently generated by UV light excitation through a biphotonic photoionization. The radical cation ***t*An**$^{\bullet+}$ was observed by nanosecond laser flash photolysis (LFP, 308 nm or 266 nm excitation) by its excited state absorptions at 320–390 nm and 520–660 nm (Murphy, et al., 2000; Johnston and Schepp, 1993). The radical cation ***t*An**$^{\bullet+}$ stabilized with $[FeCl_4]^-$ had even been isolated and an absorption band at 580 nm had been reported (Horibe, et al., 2019). Other methoxy-substituted aromatic radical cations prepared by oxidation with $MoCl_5$ were successfully characterized by EPR spectroscopy (Leppin, et al., 2015; Schubert, et al., 2016). In the $Cr^{III}$ or $Ru^{II}$ photocatalyzed reactions, the radical cations ***t*An**$^{\bullet+}$**/DAP**$^{\bullet+}$ were not yet identified spectroscopically (Stevenson, et al., 2015; Higgins, et al., 2016; Lin, et al., 2011; Farney, et al., 2019).

For $Cr^{III}$ photocatalysts and organic thioxanthylium and benzothiadiazole photocatalysts (Tanaka, et al., 2020; Huber, et al., 2020), oxygen is required for the regeneration of the reduced photocatalyst **PC**$^{(n-1)+}$ (**Scheme 1A**, mediator cycle). Interestingly, Rappé and Shores suggested that singlet oxygen $^1O_2$ is required to regenerate the chromium(III)-based **PC**$^{3+}$ forming superoxide $O_2^{\bullet-}$, which in turn reduces the cyclohexenyl radical **DAP**$^{\bullet+}$ (**Scheme 1A**) (Higgins, et al., 2016) According to the suggested mechanism, $^1O_2$ forms in a separate energy transfer photocycle (**Scheme 1A**, photocycle #2) so that two photons would be required for a single turnover. The requirement for the $O_2^{\bullet-}/^1O_2$ couple instead of the conventional redoxcouple $O_2^{\bullet-}/^3O_2$ was invoked by the negative redox potential of the latter ($E_{½}$ = −1.29 V vs. ferrocene in $CH_3CN$) (Singh and Evans, 2006), which would be insufficient for photocatalyst regeneration (Higgins, et al., 2016). In contrast to $Cr^{III}$ photocatalysts requiring $O_2$, ruthenium(II)-based photocatalysts seem to operate via a chain mechanism without the need for invoking $^1O_2$ (Lin, et al., 2011) and even in the absence of oxygen (Farney, et al., 2019).

Under photolysis conditions, $Cr^{III}$ and $Ru^{II}$ complexes of bipyridine-type ligands are photolabile (Maestri, et al., 1976; Jamieson, et al., 1979; Constable, et al., 2014; Soupart, et al., 2020; Limburg, et al., 2016). Ligand loss is observed under irradiation, forming e.g., $[(\mu\text{-}OH)_2(Cr(bpy)_2)_2]^{4+}$ (bpy = 2,2′-bipyridine) (Otto, et al., 2015; Otto, et al., 2018). Reduced complexes such as $[Cr(Ph_2phen)_3]^{2+}$ furthermore were reported to decompose in the presence of $O_2$ to Cr=O species ($Ph_2phen$ = 4,7-diphenyl-1,10-phenanthroline) (Higgins, et al., 2016). In contrast, $Cr^{III}$ complexes with tridentate ligands, in particular those inducing a very strong ligand field by large bite angles, are highly photostable, often strongly luminescent with very high excited state lifetimes, and are hence called "molecular rubies" (Otto, et al., 2015; Otto, et al., 2018b; Jiménez, et al., 2019; Treiling, et al., 2019; Reichenauer, et al., 2021). The long-lived excited states of the molecular rubies are metal-centered spin-flip states (doublet states, $^2E/^2T_1$) in contrast to the typically exploited triplet MLCT excited states of $Ru^{II}$ or $Ir^{III}$ complexes (Kitzmann, et al., 2022). Important prerequisites for the high lifetime and the photostability of molecular rubies are the large ligand field splitting resulting in dissociative metal-centered quartet states ($^4T_2$) being shifted to high energy and fast intersystem crossing (ISC) processes that rapidly depopulate the $^4T_2$ states to arrive at the long-lived $^2E/^2T_1$ states with high efficiency and without detrimental back-ISC processes (Otto, et al., 2018a; Kitzmann, et al., 2022). Potential disadvantages of the molecular rubies for photoredox applications are their comparably small extinction coefficients in the visible spectral region due to the Laporte-forbidden nature of the $^4A_2 \rightarrow {}^4T_2$ excitation and the comparably low excited state energies (1.6–1.75 eV) (Otto, et al., 2018b; Kitzmann, et al., 2022).

In the present study we explore the $Cr^{III}$ photocatalysts **[Cr(ddpd)$_2$]$^{3+}$** and **[Cr(tpe)$_2$]$^{3+}$** (**Scheme 1B**, ddpd = *N*,*N*′-dimethyl-*N*,*N*′-dipyridin-2-ylpyridine-2,6-diamine, tpe = 1,1,1-tris(pyrid-2-yl)ethane; Otto, et al., 2015; Treiling, et al., 2019) with the strong field ligands ddpd and tpe, respectively, as potential photostable photocatalysts **PC**$^{3+}$ for the visible light-

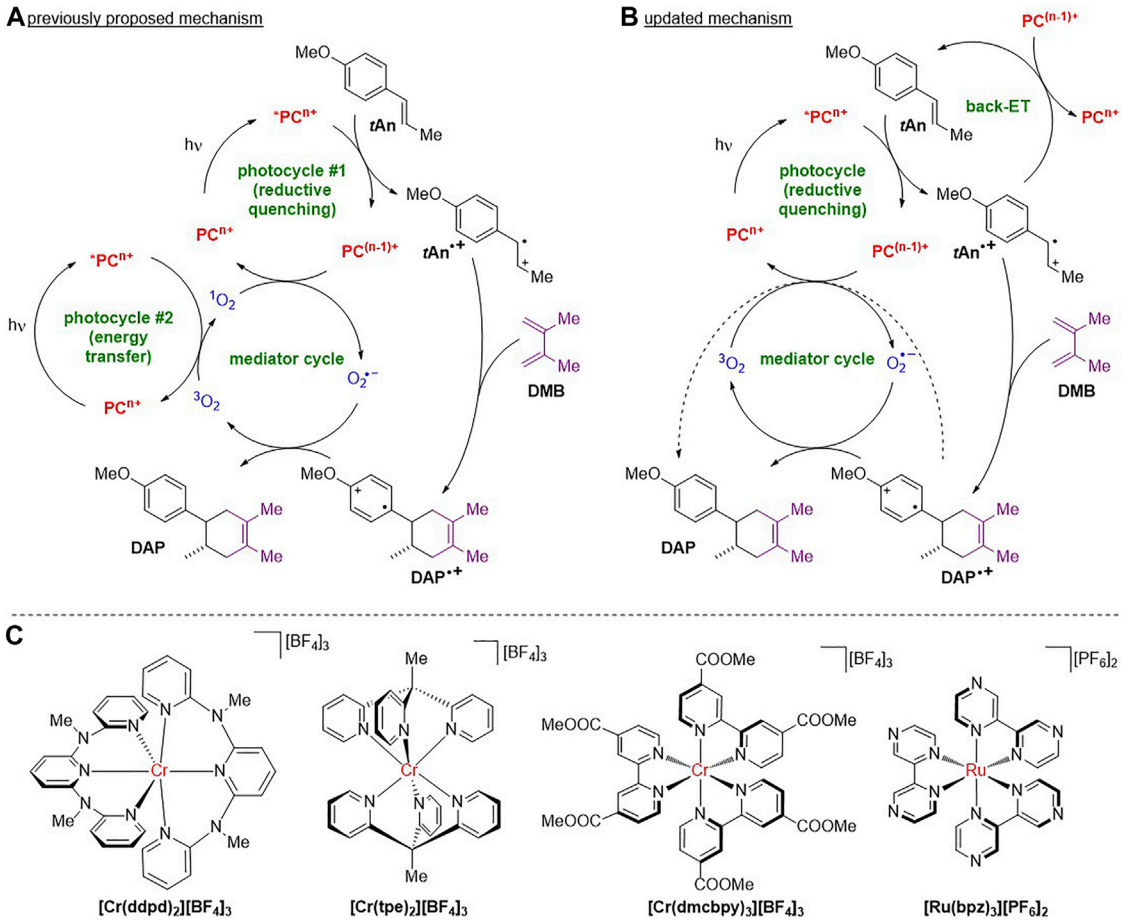


**SCHEME 1 | (A)** Previously postulated mechanism of the visible light-driven radical cation [4+2] cycloaddition of *trans*-anethole (***t*An**) and 2,3-dimethyl-1,3-butadiene (**DMB**, displayed as *s-cis* conformer) with chromium(III) photocatalyst $\mathbf{PC^{3+}}$ $\mathbf{[Cr(dmcbpy)_3]^{3+}}$ (n = 3) to the Diels-Alder product **DAP**. **(B)** Updated outline of the catalytic cycle. **(C)** Chromium(III) and ruthenium(II) photocatalysts $\mathbf{PC^{n+}}$ employed in this study.

driven radical cation [4+2] cycloaddition of ***t*An** and **DMB** (460 nm). We compare the performance with the reported optimized photocatalysts $\mathbf{[Cr(dmcbpy)_3]^{3+}}$ and $\mathbf{[Ru(bpz)_3]^{2+}}$ (bpz = 2,2′-bipyrazine; Crutchley, et al., 1980; Schultz, et al., 2015) and we investigate the role of oxygen for the regeneration of the $Cr^{III}$ photocatalysts $\mathbf{PC^{3+}}$ using nanosecond LFP studies to arrive at an updated mechanistic picture of the $Cr^{III}$ photocatalyzed radical cation Diels-Alder cycloaddition (**Scheme 1B**). Finally, we discuss the relevance and importance of extinction coefficients and photostability of the photocatalysts $\mathbf{PC^{3+}}$ and detrimental back-electron transfer processes laying the foundation for exploiting stable molecular rubies in forthcoming efficient photoredox reactions.

## EXPERIMENTAL DETAILS

**General.** The photocatalysts $\mathbf{[Cr(ddpd)_2][BF_4]_3}$ (Otto, et al., 2015; Wang, et al., 2022), $\mathbf{[Cr(tpe)_2][BF_4]_3}$ (Treiling, et al., 2019) and $\mathbf{[Cr(dmcbpy)_3][BF_4]_3}$ (McDaniel, et al., 2010) were prepared according to literature procedures. 2,3-Dimethyl-1,3-butadiene (**DMB**, 98%, Sigma-Aldrich with 100 ppm 3,5-di-*tert*-butyl-4-hydroxytoluene as stabilizer) was distilled prior to use. $\mathbf{[Ru(bpz)_3][PF_6]_2}$ (≥95%, Sigma-Aldrich), *trans*-anethole (***t*An**, 99%, Sigma), naphthalene (99%, Acros), $CH_3CN$ for photoreactions (VWR Chemicals, HPLC grade), $CH_3CN$ for spectroscopy (Supelco, hypergrade) and $CD_3CN$ (98.5% D, Deutero) were commercially available and used as received.

UV/Vis absorption spectra were recorded on a *Jasco V770* spectrometer using conventional 1.0 cm quartz cells for studies under air and 1.0 cm quartz cells with a Schott valve for studies under inert atmosphere. Emission spectra and luminescence decay curves were recorded with a FLS1000 spectrometer from *Edinburgh Instruments* equipped with the cooled red and NIR sensitive photomultiplier detectors PMT-980 and N-G09 PMT-1700, together covering the spectral range between 200 and 1700 nm. A xenon arc lamp Xe2 (450 W) was used for excitation in steady-state measurements. Time-resolved luminescence experiments on microsecond to millisecond timescale were performed in the multi-channel scaling mode employing the µs-xenon-flashlamp µF2 (pulse width ca. 2 µs) as excitation source. Measurements on the nanosecond timescale

were conducted in the TCSPC mode using a SUPERK FIANUM laser FIU-6 from *NKT Photonics* as excitation source. Absolute luminescence quantum yields $\Phi$ were determined using an integrating sphere from *Edinburgh Instruments*. Relative uncertainty of $\Phi$ is estimated to be ±10%. Stern-Volmer studies with oxygen were performed in a long-neck quartz cuvette sealed with a septum. After purging the sample solutions for about 30 min with Argon using a cannula, the emission decay was measured and the resulting lifetime was used as starting point for the Stern-Volmer analysis. To increase the oxygen partial pressures $p_{O2}$ stepwise, air was added successively to the cuvette via a syringe until air-saturation is reached. After each addition, the solution was shaken for about 2 min. The corresponding $p_{O2}$ has been determined employing the fiber-optic oxygen meter FireSting-O2 equipped with the solvent resistant probe tip OXSOLV-PT from *pyroscience*. The fiber of the probe is covered with a 150 mm cannula allowing it to pierce the septum without damaging the sensor. The sensor has been calibrated with deaerated and air-saturated solution. To assure that the $p_{O2}$ is identical during the oxygen addition and the corresponding emission decay measurement, the emission decay was always recorded after the determination of $p_{O2}$ as small amounts of air are brought into the cuvette with the cannula and are dissolved in the solution. Transient absorption spectroscopy experiments were conducted using a LP980KS setup from *Edinburgh Instruments* equipped with a Nano LG 300-10 Nd:YAG laser from *Litron* (ca. 5 ns pulse width). The frequency-tripled output with a wavelength of 355 nm was employed for the excitation (30 mJ pulse energy). To ensure homogeneous excitation of the whole observation volume (10 mm × 10 mm quartz cuvette) the beam was brought to a diameter of 1.2 cm using a beam expander. A pulsed Xe-lamp from *Hamamatsu* (150 W, XBO) was used as probe light source. The transient absorption spectra were recorded with an integration time of 100 ns using an iCCD camera from *Andor*. For the detection of the decay traces at single wavelengths a photomultiplier tube was employed. All transient absorption experiments were performed at 293 K. $^1$H NMR spectra were recorded on a Bruker Avance II 400 spectrometer at 400.13 MHz. All resonances are reported in ppm versus the solvent signal as an internal standard (δ = 1.94, $CD_3CN$) (Fulmer, et al., 2010).

General Procedure for the light-driven radical cation [4+2] cycloaddition. A solution of *trans*-anethole ***t*An** (100 mM), 2,3-dimethyl-1,3-butadiene **DMB** (500 mM) and the photocatalyst (0.2–5 mM) in acetonitrile with a total volume of 2 ml was prepared in a 4 ml vial. The vial was capped with a septum, pierced with a needle to allow air contact, equipped with a stir bar and placed in an Aldrich® Micro Photochemical Reactor (16 vial places) equipped with blue LEDs (for the LED emission spectrum in combination with the UV/Vis absorption spectra of the photocatalysts see **Supplementary Figures S1–S4**). The vials were irradiated at 294 K. The progress of the reaction was monitored by $^1$H NMR spectroscopy. To this end an aliquot of the reaction mixture was taken and added to a solution of an internal standard (naphthalene) in $CD_3CN$. The yield was determined via integration of the product and starting material resonances versus the internal standard.

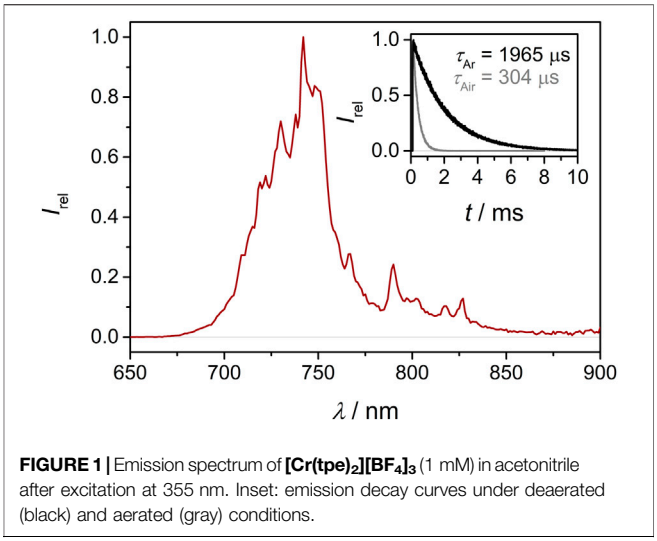


**FIGURE 1 |** Emission spectrum of **[Cr(tpe)$_2$][BF$_4$]$_3$** (1 mM) in acetonitrile after excitation at 355 nm. Inset: emission decay curves under deaerated (black) and aerated (gray) conditions.

Isolation of the product DAP. In order to isolate the **DAP** product, water (2 ml) was added to the reaction mixture and the solution was extracted with diethylether (2 × 2 ml). The organic phase was dried over anhydrous sodium sulfate and the solvent was removed under reduced pressure. The crude product was purified by filtration through a silica-filled glass pipette using cyclohexane. The solvent was removed under reduced pressure to give the product as a colorless oil.

## RESULTS AND DISCUSSION

The photocatalysts **[Cr(ddpd)$_2$]$^{3+}$**, **[Cr(tpe)$_2$]$^{3+}$**, **[Cr(dmcbpy)$_3$]$^{3+}$** and **[Ru(bpz)$_3$]$^{2+}$** (**PC$^{n+}$**) employed in this study are depicted in **Scheme 1C** (Otto, et al., 2015; Treiling, et al., 2019; Crutchley and Lever, 1980). All complexes absorb blue light with absorption maxima at 436, 431, 448 and 440 nm in $CH_3CN$, albeit with very different extinction coefficients of $\varepsilon_{max}$ = 3770, 30, 714 and 14,100 $M^{-1}$ $cm^{-1}$, respectively. Excitation with blue light leads to phosphorescence emission maxima at 776, 748, 733 and 607 nm, respectively. Under inert atmosphere, the corresponding excited state lifetimes amount to 1136, 1965, 25 and 0.762 µs (**Figure 1**; **Supplementary Figures S5–S7**) and the photoluminescence quantum yields to 12.1, 4.0, 0.14 and 6.5%, respectively.

Thermodynamically, all chromium(III) complexes **[Cr(ddpd)$_2$]$^{3+}$**, **[Cr(tpe)$_2$]$^{3+}$** and **[Cr(dmcbpy)$_3$]$^{3+}$** as well as **[Ru(bpz)$_3$]$^{2+}$** can sensitize triplet oxygen ($^3O_2$) to give singlet oxygen ($^1O_2$) due to their excited state energies (1.6–2.16 eV; Otto, et al., 2015; Treiling, et al., 2019; Stevenson, et al., 2015; Vleck, et al., 1995) exceeding the energy of $^1O_2$ (0.97 eV). In aerated $CH_3CN$ solution, the luminescence lifetimes decrease to 48, 304, 19 and 0.561 µs for **[Cr(ddpd)$_2$]$^{3+}$**, **[Cr(tpe)$_2$]$^{3+}$**, **[Cr(dmcbpy)$_3$]$^{3+}$** and **[Ru(bpz)$_3$]$^{2+}$**, respectively (**Figure 1**; **Supplementary Figures S5–S7**). **[Cr(ddpd)$_2$]$^{3+}$** had been employed for $^1O_2$ generation for the α-cyanation of aliphatic amines and in biological environments (Otto, et al., 2015; Otto,

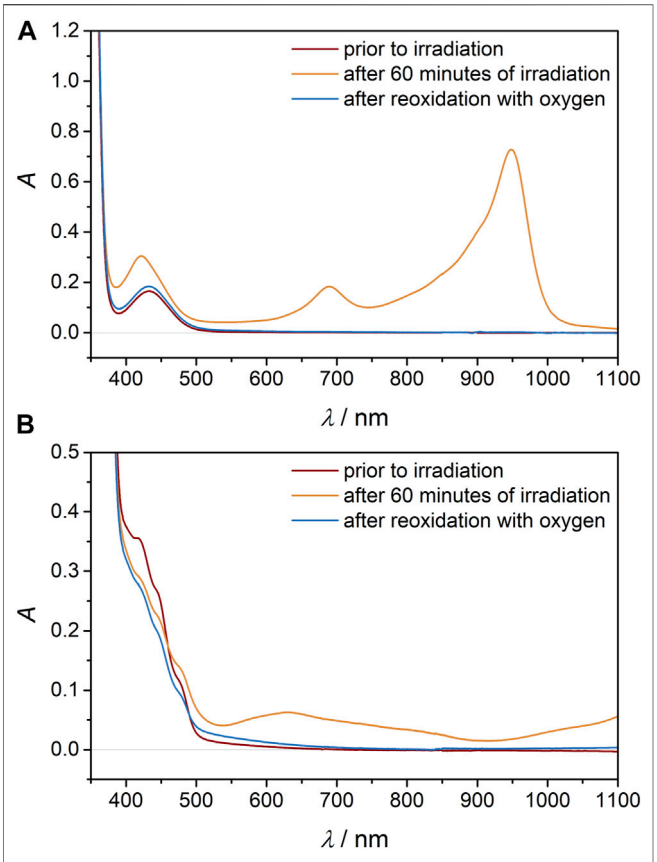


**FIGURE 2 |** UV/vis/NIR absorption spectra of **(A)** $[Cr(tpe)_2]^{3+}$ and **(B)** $[Cr(dmcbpy)_3]^{3+}$ in $CH_3CN$ prior to irradiation (red), after 60 min of LED irradiation ($\lambda_{exc}$ = 460 nm) under argon in the presence of ***t*An** (orange) and after re-oxidation with air in the dark (blue).

et al., 2017; Basu, et al., 2019). The spin-flip phosphorescence of $[Cr(tpe)_2]^{3+}$ is likewise quenched by $O_2$ (Treiling, et al., 2019). Stern-Volmer studies of $[Cr(ddpd)_2]^{3+}$, $[Cr(tpe)_2]^{3+}$, $[Cr(dmcbpy)_3]^{3+}$ and $[Ru(bpz)_3]^{2+}$ with $O_2$ in $CH_3CN$ yield $K_{SV} = 130 \times 10^{-3}$, $34 \times 10^{-3}$, $1.8 \times 10^{-3}$ and $2.3 \times 10^{-3}$ $hPa^{-1}$ and $k_q$ = 115, 17.3, 73.3 and 3010 $hPa^{-1}\,s^{-1}$, respectively (**Supplementary Figures S8–S11**). The concentration of $^3O_2$ in air-saturated $CH_3CN$ solution has been reported as 1.9 mM (Montalti, et al., 2006). The formation of $^1O_2$ was confirmed by its characteristic emission band at 1275 nm (**Supplementary Figure S12**). Its experimental formation and decay was excellently reproduced by a kinetic model shown in the Supplementary Material (**Supplementary Figure S12**). As $^1O_2$ is formed and sufficiently long-lived, it might play a role in the catalytic cycle as proposed by Rappé and Shores (**Scheme 1A**), although its concentration would be quite low (Higgins, et al., 2016). Even in the presence of oxygen, the excited state lifetimes of $[Cr(ddpd)_2]^{3+}$, $[Cr(tpe)_2]^{3+}$, $[Cr(dmcbpy)_3]^{3+}$ and $[Ru(bpz)_3]^{2+}$ remain high (**Figure 1**; **Supplementary Figures S5–S7**) enabling efficient quenching with other substrates in parallel processes such as photoinduced redox processes.

Indeed, the chromium(III) complexes $[Cr(ddpd)_2]^{3+}$, $[Cr(tpe)_2]^{3+}$ and $[Cr(dmcbpy)_3]^{3+}$ can be reduced to the corresponding dications at −1.11, −0.88 and −0.26 V vs. ferrocene, respectively (Otto, et al., 2015; Treiling, et al., 2019; McDaniel, et al., 2010). The ruthenium(II) complex $[Ru(bpz)_3]^{2+}$ can be reduced at −1.11 V whereby the additional electron occupies a ligand-centered π* orbital (Campagna, et al., 2007; Balzani, et al., 1978). Reduced chromium(III) complexes are either genuine chromium(II) complexes for electron-rich ddpd ligands (Becker, et al., 2020) or ligand centered radicals for electron-deficient tpe, bpmp or bpy-type ligands (bpmp = 2,6-bis(2-pyridylmethyl)pyridine; Treiling, et al., 2019; Reichenauer, et al., 2020; Scarborough, et al., 2011). While metal-centered reduction to $Cr^{II}$ can labilize ligands, ligand-centered radicals appear comparably stable similar to ligand-reduced ruthenium(II) complexes such as $[Ru(bpz)_3]^{+}$ (Campagna, et al., 2007; Balzani, et al., 1978; Lin, et al., 2011).

$[Cr(bpy)_3]^{3+}$, $[Cr(tpy)_2]^{3+}$ and related derivatives photooxidize DNA via initial guanine base oxidation (tpy = 2,2'; 6′,2″-terpyridine) while $^*[Cr(ddpd)_2]^{3+}$ does not oxidize guanine bases due to its low excited state redox potential $E_{½}([^*Cr(ddpd)_2]^{3+}/[Cr(ddpd)_2]^{2+})$ = 0.49 V(Baptista, et al., 2021; Watson, et al., 1999; Vaidyanathan, et al., 2004; Otto, et al., 2015). We will exploit the selectivity of $^*[Cr(ddpd)_2]^{3+}$ for energy transfer over electron transfer later in mechanistic studies (Otto, et al., 2015). On the other hand, the excited state potentials of $[Cr(tpe)_2]^{3+}$ and $[Cr(dmcbpy)_3]^{3+}$ of 0.87 and 1.44 V approach or even exceed that of $[Ru(bpz)_3]^{2+}$ with 0.99 V. Hence, $[Cr(tpe)_2]^{3+}$, $[Cr(dmcbpy)_3]^{3+}$ and $[Ru(bpz)_3]^{2+}$ are strong photooxidants capable of oxidizing ***t*An** to $t\mathbf{An}^{\bullet+}$ ($E_{½}$ = 0.78 V; Higgins, et al., 2016), while $[Cr(ddpd)_2]^{3+}$ is thermodynamically incompetent for this photoredox reaction. Consequently, ***t*An** reductively quenches the emission of $[Cr(tpe)_2]^{3+}$, $[Cr(dmcbpy)_3]^{3+}$ and $[Ru(bpz)_3]^{2+}$ but not that of $[Cr(ddpd)_2]^{3+}$. Stern-Volmer and quenching rate constants of $[Cr(tpe)_2]^{3+}$, $[Cr(dmcbpy)_3]^{3+}$ and $[Ru(bpz)_3]^{2+}$ with ***t*An** were determined as $K_{SV}$ = 4500, 75,000 and 740 $M^{-1}$ and $k_q$ = $2.3\times10^6$, $3000\times10^6$ and $970\times10^6$ $M^{-1}\,s^{-1}$, respectively (**Supplementary Figures S13–S15**). The different rates reflect the different driving forces for the electron transfer from ***t*An** to the excited photocatalyst $^*PC^{n+}$ (Marcus, 1993). $[Cr(tpe)_2]^{2+}$ forms by reduction of $[Cr(tpe)_2]^{3+}$ with ***t*An** under light irradiation in the photo reactor as confirmed by UV/Vis spectroscopy and comparison with an authentic spectrum (**Figure 2A**) (Treiling, et al., 2019) Similarly $[Cr(dmcbpy)_3]^{3+}$ is reduced to $[Cr(dmcbpy)_3]^{2+}$ (**Figure 2B**) by reference to spectra of $[CrL_3]^{2+}$ complexes with bpy-type ligands (Scarborough, et al., 2011; Higgins, et al., 2016).

Interestingly, addition of $O_2$ to the $[Cr(tpe)_2]^{2+}$ solution in the dark restores the UV/vis/NIR absorption spectrum of $[Cr(tpe)_2]^{3+}$ quantitatively demonstrating that $^3O_2$ can oxidize $[Cr(tpe)_2]^{2+}$ to $[Cr(tpe)_2]^{3+}$ (**Figure 2A**). Similarly, the UV/vis/NIR absorption spectrum of $[Cr(dmcbpy)_3]^{3+}$ is recovered by addition of $O_2$ to the $[Cr(dmcbpy)_3]^{3+}$ solution in the dark at least to a large extent (**Figure 2B**). This points to some instability either of $[Cr(dmcbpy)_3]^{2+}$ or the photoexcited complex $^*[Cr(dmcbpy)_3]^{3+}$. In fact, $[Cr(tpe)_2]^{3+}$ is photostable in $CH_3CN$ over several days of irradiation while $[Cr(dmcbpy)_3]^{3+}$ and $[Ru(bpz)_3]^{2+}$ partially decompose over time

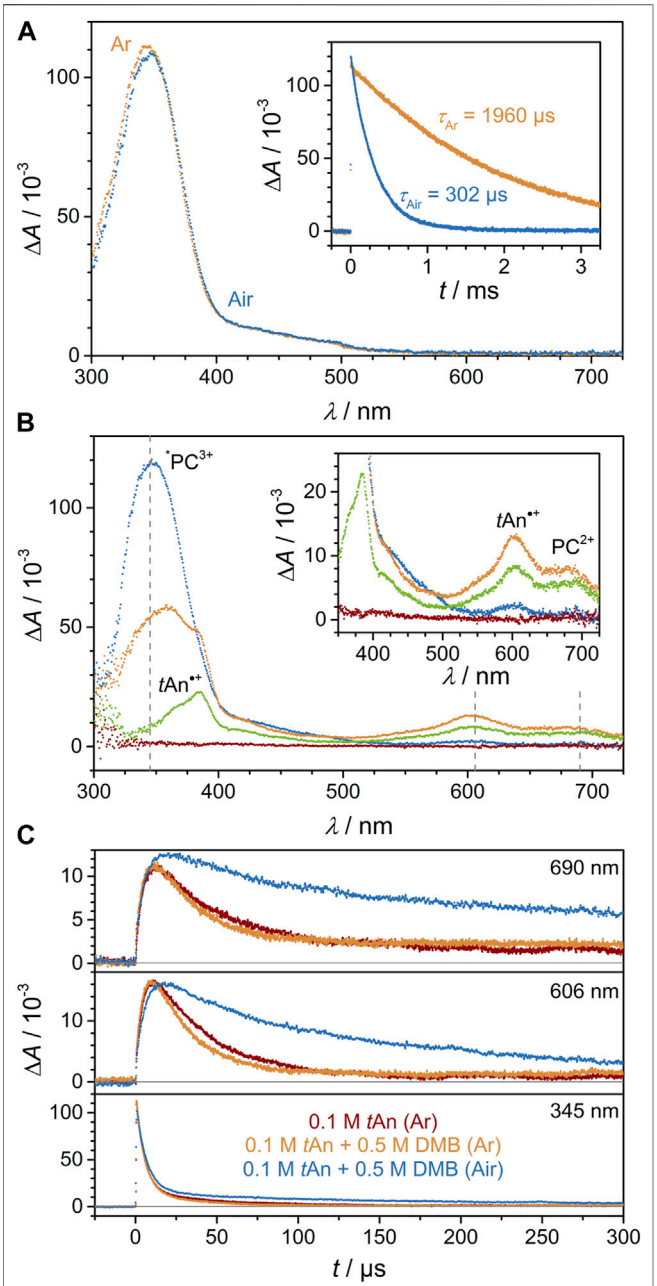


**FIGURE 3 |** LFP investigations on pure and quenched solutions of **[Cr(tpe)$_2$][BF$_4$]$_3$** (0.35 mM) in acetonitrile illustrating the evolution and the decay of the key intermediates ***PC$^{3+}$**, **PC$^{2+}$** and ***t*An$^{•+}$** following laser excitation at 355 nm. **(A)** Transient absorption spectra of an air-saturated (blue) and a deaerated (orange) **[Cr(tpe)$_2$][BF$_4$]$_3$** solution at a time delay of 50 ns. Inset, corresponding decay traces at 345 nm. **(B)** Transient absorption spectra monitored 50 ns (blue), 5 µs (orange), 50 µs (green) and 500 µs (red) after laser excitation of a deaerated **[Cr(tpe)$_2$][BF$_4$]$_3$** solution in acetonitrile quenched by 0.1 M ***t*An**. **(C)** Decay traces at 345, 606 and 690 nm upon excitation of **[Cr(tpe)$_2$][BF$_4$]$_3$** solutions with 0.1 M ***t*An** (deaerated, red) and 0.1 M ***t*An** and 0.5 M **DMB**, respectively (deaerated, orange; air-saturated, blue).

irrespective of the presence or absence of $O_2$ (**Supplementary Figures S16–S21**). The recovery of **[Cr(tpe)$_2$]$^{3+}$** and **[Cr(dmcbpy)$_3$]$^{3+}$** by oxygen in the absence of light clearly demonstrates that in contradiction to the previously proposed mechanism no $^1O_2$ is needed to reoxidize the catalyst. This surprising finding motivated us to perform LFP investigations on **[Cr(tpe)$_2$]$^{3+}$** to unravel the mechanism and importantly to elucidate the role of oxygen in this photoredox catalytic cycle.

A solution of **[Cr(tpe)$_2$]$^{3+}$** in deaerated acetonitrile was excited at 355 nm. **Figure 3A** illustrates the resulting transient absorption spectrum, which is dominated by a strong positive absorption band centered at 345 nm. According to time-dependent Density Functional Theory calculations, this absorption band covers spin-allowed transitions with doublet ligand-to-metal and intraligand character calculated at 345 and 373 nm (**Supplementary Tables S1, S2**). Analogous quartet transitions are calculated at 325 nm for the quartet ground state. The assignments fit to the observed experimental band maxima of 329 nm (**Supplementary Figure S3**) and 345 nm for **$^4$[Cr(tpe)$_2$]$^{3+}$** and **$^2$[Cr(tpe)$_2$]$^{3+}$**, respectively. The decay trace observed at 345 nm for **$^2$[Cr(tpe)$_2$]$^{3+}$** shows a first order decay with a time constant of 1960 µs. In air-saturated solution the absorption spectrum remains unaltered, but the lifetime substantially decreases to 302 µs, compared to the deaerated solution. Both lifetimes excellently agree with the emission lifetimes determined via time-resolved emission (**Figures 1**, **3A**).

Excitation of a deaerated solution of **[Cr(tpe)$_2$]$^{3+}$** in the presence of 0.1 M ***t*An** initially yields the same absorption spectrum as the photocatalyst alone showing that no observable intermediates are formed due to direct excitation of ***t*An** (**Figure 3B**). The ***PC$^{3+}$** absorption (345 nm) rapidly decays with a lifetime of *ca.* 5 µs (**Figure 3C**), which agrees with the time constant found for the emission quenching (**Supplementary Figure S14**, $\tau_0$ = 1965 µs, $K_{SV}$ = 4520 M$^{-1}$, 0.1 M ***t*An**). Two new bands appear at 385 and 606 nm (**Figure 3B**) that coincide with the absorption maxima reported for ***t*An$^{•+}$** by Johnston and Schepp (Johnston and Schepp, 1993) confirming the formation of the radical cation by reductive quenching of ***PC$^{3+}$**. An additional weak band was observed at 690 nm that can be assigned to **PC$^{2+}$** by comparison with an authentic spectrum (**Figure 2A**; Treiling, et al., 2019), albeit ***t*An$^{•+}$** also significantly contributes to the absorption at this wavelength. **Figure 3C** (red curves) displays the decay traces at the absorption maxima 345, 606 and 690 nm, corresponding to ***PC$^{3+}$**, ***t*An$^{•+}$** and **PC$^{2+}$**, respectively. Interestingly, the kinetic traces at 606 and 690 nm show a first-order decay with a lifetime of *ca.* 45 µs (first measurement with a fresh sample) after an initial rise period of approximately 20 µs. This finding is unexpected for two reasons: the radical cation ***t*An$^{•+}$** is much more long-lived than described by Johnston and Schepp (Johnston and Schepp, 1993) and the unproductive non-geminate back-electron transfer (back-ET) from **PC$^{2+}$** to ***t*An$^{•+}$** should be the dominant deactivation process in the absence of oxygen or **DMB**, which would yield a second-order decay. This deviation from the expected second-order rate law can be rationalized by a build-up of **PC$^{2+}$** during the LFP experiment, which can lead to pseudo-first order kinetics. Although **PC$^{2+}$** and ***t*An$^{•+}$** are initially formed in equal amounts, **PC$^{2+}$** can accumulate by removing a fraction of ***t*An$^{•+}$** via a side reaction. In fact, ***t*An$^{•+}$** is known to undergo a variety of reactions besides back electron transfer, e.g. addition to

***t*An**, nucleophilic addition and dimerization (Johnston and Schepp, 1993; Johnston and Schepp 1995). In principle, the addition of $t\mathbf{An}^{\bullet+}$ to ***t*An** alone could also explain the observed pseudo first-order rate law. However, only traces of side products were observed upon irradiation with a LED, which reveals that only a small fraction of $t\mathbf{An}^{\bullet+}$ follows this reaction path. Yet this small amount of removed $t\mathbf{An}^{\bullet+}$ would suffice to explain the accumulation of $\mathbf{PC}^{2+}$ as the ***t*An** concentration exceeds the concentration of $[\mathbf{Cr(tpe)_2}]^{3+}$ by approximately two orders of magnitude. The substantial residual signal at 690 nm provides further evidence for this incomplete reoxidation of $\mathbf{PC}^{2+}$ to $\mathbf{PC}^{3+}$. In order to test whether $\mathbf{PC}^{2+}$ accumulates during the LFP experiments, we performed repeated measurements of the decay trace at 606 nm (eight iterations) with the same sample. In this series of experiments the lifetime successively decreases to a limiting value of 23 µs (**Supplementary Figure S22**). Moreover, the static UV/vis/NIR spectrum recorded after the LFP measurement clearly shows the characteristic spectral signature of $\mathbf{PC}^{2+}$ (**Supplementary Figure S23**).

In order to observe the [4+2] cycloaddition step of $t\mathbf{An}^{\bullet+}$ to **DMB** to give $\mathbf{DAP}^{\bullet+}$ (**Scheme 1B**), LFP measurements were conducted with additional 0.5 M **DMB**. However, the obtained transient absorption spectra in the presence and absence of **DMB** are basically identical (**Supplementary Figure S24**). Consequently, the formation of $\mathbf{DAP}^{\bullet+}$ cannot be monitored under these conditions. **Figure 3C** (orange curve) illustrates the corresponding decay traces. Despite of the large excess of **DMB**, the decay rate observed at 606 nm ($t\mathbf{An}^{\bullet+}$) and 690 nm ($\mathbf{PC}^{2+}$) is only slightly increased. The very slow kinetics might be explained by the preferred *s-trans* conformation (by 8.3 kJ $mol^{-1}$; Squillacote and Liang, 2005) of **DMB** and the steric demands of the diene **DMB** and the dienophile $t\mathbf{An}^{\bullet+}$ posing a barrier for the addition/cyclization step to $\mathbf{DAP}^{\bullet+}$. This argument also rationalizes the missing accumulation of $\mathbf{DAP}^{\bullet+}$. Hence, the slow [4+2] cycloaddition of **DMB** with $t\mathbf{An}^{\bullet+}$ is probably the bottleneck of the reaction sequence. In agreement with this interpretation, the first C–C bond formation of the asynchronous radical cation [4+2] cycloaddition has been identified computationally to be the most demanding step (Young, et al., 2017).

Finally, LFP measurements were performed on an air-saturated solution of $[\mathbf{Cr(tpe)_2}]^{3+}$, 0.1 M ***t*An** and 0.5 M **DMB**. The shape of the absorption spectra remains unaffected by the presence of oxygen (**Supplementary Figure S25**). Surprisingly, the presence of oxygen strongly *prolongs* the lifetime of $t\mathbf{An}^{\bullet+}$ (**Figure 3C**, blue curves). This contrasts the reported reaction of $t\mathbf{An}^{\bullet+}$ (prepared by direct photoionization at 308 or 266 nm) with $O_2$ (Johnston and Schepp, 1993), which *shortens* the lifetime significantly ($k_{O2}$ = $2.3\times10^7$ $M^{-1}s^{-1}$). The decay of $t\mathbf{An}^{\bullet+}$ (prepared by photoinduced electron transfer to $\mathbf{PC}^{3+}$) in the presence of $O_2$ can be reasonably well described with second order kinetics (**Supplementary Figure S26**) in contrast to the first order decay found for the Ar-saturated samples. We surmise that $^3O_2$ oxidizes $\mathbf{PC}^{2+}$ recovering the catalyst in its initial form, which prevents the accumulation of $\mathbf{PC}^{2+}$ during the LFP measurement and also during the continuous irradiation in the laboratory scale experiments. Consequently, the non-geminate back-ET from $\mathbf{PC}^{2+}$ to $t\mathbf{An}^{\bullet+}$ is slowed down by the removal of $\mathbf{PC}^{2+}$ with $O_2$, which enhances the lifetime of $t\mathbf{An}^{\bullet+}$. Interestingly, the lifetime of $t\mathbf{An}^{\bullet+}$ further increases, when the decay trace at 606 nm is repeatedly recorded with the same sample but stays constant after the sixth iteration (**Supplementary Figure S26**). This observation might be explained by photochemical self-cleaning, which removes trace impurities in the catalyst solution.

In summary, the collected data support the simplified productive mechanistic picture outlined in **Scheme 1B**. This scheme includes a non-productive back-ET pathway, but lacks a second photocycle proposed in **Scheme 1A** involving $^1O_2$. Excitation of the $Cr^{III}$ photocatalyst initially yields a quartet excited state ($^4T_2$ or $^4CT$ states), which evolve to the productive doublet states via ISC. While $[\mathbf{Cr(dmcbpy)_3}]^{3+}$ suffers from occasional photodissociation, $[\mathbf{Cr(tpe)_2}]^{3+}$ is stable towards photodissociation and photosubstitution. Both complexes can form $^1O_2$ from $^3O_2$ in their long-lived excited doublet states but with comparably low efficiency. In fact, our studies clearly demonstrate that $^1O_2$ is unnecessary to regenerate $\mathbf{PC}^{3+}$ from $\mathbf{PC}^{2+}$ as $^3O_2$ is already competent in spite of its formal reduction potential being very negative (Singh, et al., 2006). Hydrogen-bond forming water has been reported to shift the $O_2^{\bullet-}/^3O_2$ potential to less negative values and protonation of $O_2^{\bullet-}$ to $HO_2^{\bullet}$ might even drive the redox reaction due to $O_2^{\bullet-}$ consumption, which might explain the $\mathbf{PC}^{n+}$ regeneration competency of the $O_2^{\bullet-}/^3O_2$ pair in non-dried $CH_3CN$ (Singh, et al., 2006). Consequently, $^1O_2$ as proposed in **Scheme 1A** is not mandatory for the productive catalytic cycle (**Scheme 1B**). Reductive quenching of the long-lived excited doublet states of $\mathbf{PC}^{3+}$ by the styrene ***t*An** is highly efficient forming the reduced photocatalyst $\mathbf{PC}^{2+}$ and the radical cation $t\mathbf{An}^{\bullet+}$. In the absence of $O_2$, $\mathbf{PC}^{2+}$ can recombine with $t\mathbf{An}^{\bullet+}$ in a non-productive back-ET due to the microsecond lifetime of $t\mathbf{An}^{\bullet+}$ in the absence of substrates. Even in the presence of excess **DMB**, the lifetime of $t\mathbf{An}^{\bullet+}$ exceeds microseconds suggesting that the addition of $t\mathbf{An}^{\bullet+}$ to **DMB** is the rate-determining step for the catalytic cycle. Shores and others also noticed that the cycloaddition step is slow with terminally substituted dienes but is positively influenced by the presence of $O_2$ (Higgins, et al., 2016). In the presence of $O_2$, $\mathbf{PC}^{2+}$ is re-oxidized sufficiently fast by $^3O_2$ to give $\mathbf{PC}^{3+}$ and $O_2^{\bullet-}$. The removal of $\mathbf{PC}^{2+}$ prolongs the lifetime of $t\mathbf{An}^{\bullet+}$ increasing the probability for the radical addition step. Both $\mathbf{PC}^{2+}$ and $O_2^{\bullet-}$ are thermodynamically capable to reduce the product cyclohexene radical cation $\mathbf{DAP}^{\bullet+}$ to the final product. The radical cation $\mathbf{DAP}^{\bullet+}$ is not observed by LFP neither in the presence nor absence of $O_2$ suggesting that its reduction by $\mathbf{PC}^{2+}$ is faster than its formation (**Scheme 1B**). Consequently, the main task of $O_2$ is to rapidly remove $\mathbf{PC}^{2+}$ to prevent non-geminate back-ET from $\mathbf{PC}^{2+}$ to $t\mathbf{An}^{\bullet+}$ and thus to enable the slow addition reaction of $t\mathbf{An}^{\bullet+}$ to **DMB**, while $O_2^{\bullet-}$ is not necessarily required to reduce $\mathbf{DAP}^{\bullet+}$. Furthermore, rapid regeneration of $\mathbf{PC}^{3+}$ prevents accumulation of the highly absorptive one-electron reduced photocatalyst $\mathbf{PC}^{2+}$ $[\mathbf{Cr(tpe)_2}]^{2+}$ (**Figure 2A**) which would absorb a significant amount of the incoming photons.

The competent photocatalysts $[\mathbf{Cr(tpe)_2}]^{3+}$, $[\mathbf{Cr(dmcbpy)_3}]^{3+}$ and $[\mathbf{Ru(bpz)_3}]^{2+}$ were employed in catalytic experiments with ***t*An**

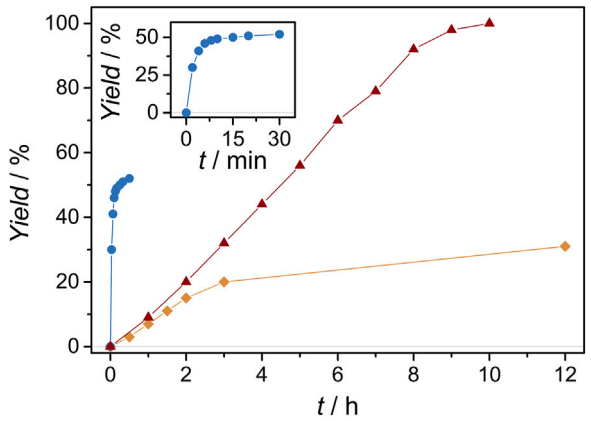


**FIGURE 4 |** Conversion vs. time plots of the photoredox catalyzed radical cation Diels-Alder cycloaddition of ***t*An** and **DMB** using **$[Cr(tpe)_2]^{3+}$** (red triangles), **$[Cr(dmcbpy)_3]^{3+}$** (orange diamonds) and **$[Ru(bpz)_3]^{2+}$** (blue circles) photocatalysts (0.2 mM) in $CH_3CN$ with 460 nm light excitation. The inset shows a zoom of the conversion vs. time plot of the rapid but incomplete reaction with **$[Ru(bpz)_3]^{2+}$** as photocatalyst.

and **DMB** substrates in air-saturated $CH_3CN$ under visible light excitation (460 nm). The overlap of the absorption spectra of $\mathbf{PC}^{n+}$ and the emission of the LEDs employed reveal that photon absorption in this spectral region increases in the series $[Cr(tpe)_2]^{3+}$, $[Cr(dmcbpy)_3]^{3+}$ and $[Ru(bpz)_3]^{2+}$ due to the weak Laporte-forbidden absorption bands of the $Cr^{III}$ photocatalysts in the visible spectral region. This is particularly concerning for the centrosymmetric complex $[Cr(tpe)_2]^{3+}$ with an extinction coefficient at its absorption maximum of only $\varepsilon_{431}$ = 30 $M^{-1}$ $cm^{-1}$ as compared to the much higher extinction coefficients of $[Cr(dmcbpy)_3]^{3+}$ ($\varepsilon_{448}$ = 714 $M^{-1}$ $cm^{-1}$) and $[Ru(bpz)_3]^{2+}$ ($\varepsilon_{440}$ = 14,100 $M^{-1}$ $cm^{-1}$). Consequently, we employed a loading of 5 mM $[Cr(tpe)_2]^{3+}$ in initial catalytic tests. According to $^1$H NMR spectroscopic reaction monitoring (**Supplementary Figures S27–S31**), full conversion to the Diels-Alder product **DAP** is achieved with $[Cr(tpe)_2]^{3+}$ within ca. 80 min (**Supplementary Figure S32**). In the absence of $O_2$ only traces of **DAP** were observed after 4 h irradiation (**Supplementary Figure S33**). Introduction of $O_2$ to this pretreated reaction mixture initiates the catalytic turnover and the reaction proceeds quantitatively. This confirms that the unproductive back-ET efficiently prevents the formation of $\mathbf{DAP}^{\bullet+}$. In the absence of light (24 h) or $[Cr(tpe)_2]^{3+}$ (24 h) **DAP** formation is not observed (**Supplementary Figures S34, S35**). In the latter case, traces of 4-anisaldehyd and other byproducts are formed (**Supplementary Figure S35**). Reducing the catalyst loading to 1 and 0.2 mM prolongs the reaction time to reach full conversion to ca. 5–6 and 9–10 h, respectively (**Figure 4**; **Supplementary Figure S36**). Notably, full conversion is achieved with $[Cr(tpe)_2]^{3+}$ in all cases. The solutions remain only weakly colored during the photolysis experiments suggesting a high stability of $[Cr(tpe)_2]^{3+}$, $^*[Cr(tpe)_2]^{3+}$ and $[Cr(tpe)_2]^{2+}$. In fact, addition of new ***t*An** and **DMB** substrates to the catalysis solution after full conversion, resumes the catalytic activity without noticeable degradation as demonstrated two times (**Supplementary Figure S37**). The high photo and redoxstability of $[Cr(tpe)_2]^{3+}$ (**Supplementary Figure S38**) and the resulting recyclability (**Supplementary Figure S37**) are unique to $[Cr(tpe)_2]^{3+}$ (**Figure 4**).

$[Ru(bpz)_3]^{2+}$ reacts initially much faster than the $Cr^{III}$ photocatalysts $[Cr(dmcbpy)_3]^{3+}$ and $[Cr(tpe)_2]^{3+}$ with initial rates being 300 × $10^{-4}$, 2.5 × $10^{-4}$ and 4.3 × $10^{-4}$ mM $min^{-1}$ and turnover frequencies being TOF = 75, 0.6 and 1.1 $min^{-1}$, respectively (loading 0.2 mM; **Figure 4**). Importantly, $[Cr(dmcbpy)_3]^{3+}$ and $[Ru(bpz)_3]^{2+}$ do not achieve full conversion under these conditions (loading 0.2 mM) but the catalytic activity levels off at ca. 30 and 50% conversion after 720 and 6 min, respectively. Photodecomposition of the $[Cr(dmcbpy)_3]^{3+}$ and $[Ru(bpz)_3]^{2+}$ with ligand loss is likely responsible for this behavior. Indeed, the UV/Vis spectra of the solutions after the catalysis changed for $[Cr(dmcbpy)_3]^{3+}$ and $[Ru(bpz)_3]^{2+}$, but not for $[Cr(tpe)_2]^{3+}$ (**Supplementary Figures S38–S40**). Although conditions for chromium(III) and ruthenium(II) complexes with bidentate ligands can be optimized to achieve full conversion, re-using these photocatalysts has not yet been reported (Lin, et al., 2011; Stevenson, et al., 2015; Farney, et al., 2019).

Only traces of byproducts form during the reaction with $[Cr(tpe)_2]^{3+}$ as photocatalyst. Discernible $^1$H NMR resonances at δ = 9.84, 7.82, 6.87 and 3.86 ppm suggest the formation of 4-anisaldehyde arising from the reaction of $\mathbf{\textit{t}An}^{\bullet+}$ with oxygen (<< 1%; **Supplementary Figure S41**) (Lewis and Kijima, 1988) A further byproduct with $^1$H NMR resonances around 8.8 ppm also likely arises from a $\mathbf{\textit{t}An}^{\bullet+}$ derived species but could not be definitely assigned, yet various dimers and other oxygenated products are conceivable (Nozaki, et al., 1968). Side reactions of ***t*An** with $^1O_2$ are excluded as a photocatalytic control reaction using $[Cr(ddpd)_2]^{3+}$ as $\mathbf{PC}^{3+}$ which is merely capable to form $^1O_2$ but not $\mathbf{\textit{t}An}^{\bullet+}$ does not yield any products.

At first glance, molecular rubies seem to be rather unattractive in the context of photochemical applications, such as photoredox catalysis, due to their low absorbance in the visible part of the spectrum, which appears to imply an inefficient use of the incident photons. This seems especially true for $[Cr(tpe)_2]^{3+}$, which has an extinction coefficient as low as 30 $M^{-1}$ $cm^{-1}$ at the maximum of the band in the visible region. However, for one-photon processes and a reasonable reactor design, this turns out to be not the case, especially when the photocatalyst is as stable (reusable) and easy to access as $[Cr(tpe)_2]^{3+}$. Laboratory scale applications typically go hand in hand with a moderate upscaling compared to the mechanistic studies that are typically conducted in a cuvette or vial. On a preparative laboratory scale it is convenient to conduct the reaction in a round bottom flask or a larger cuvette, such an optical path of 10 cm or more is likely achieved. In this case, $[Cr(tpe)_2]^{3+}$ photocatalyst loadings of 1 and 5 mM give absorbances of 0.3 and 1.5, respectively. According to the Lambert-Beer law 50 and 97% of the incident photons are absorbed, which is a fairly efficient use of light. In fact, the low extinction coefficient of $[Cr(tpe)_2]^{3+}$ and other molecular rubies might be even beneficial in some reactions as byproduct formation can be decreased by mitigating high local concentrations of radical intermediates as opposed to reactions with strongly absorbing catalysts.

## CONCLUSION

The chromium(III)-based photocatalysts $\mathbf{PC^{3+}}$ $\mathbf{[Cr(dmcbpy)_3]^{3+}}$ and $\mathbf{[Cr(tpe)_2]^{3+}}$ catalyze the visible light-driven radical cation [4+2] cycloaddition of *trans*-anethole ***t*An** and 2,3-dimethyl-1,3-butadiene **DMB** using visible light similar to the highly oxidative ruthenium(II) photocatalyst $\mathbf{[Ru(bpz)_3]^{2+}}$. The chromium(III) photocatalysts $\mathbf{PC^{3+}}$ are quenched reductively by ***t*An** to give $\mathbf{PC^{2+}}$ and $\mathbf{\textit{t}An^{\bullet+}}$. The reaction of $\mathbf{\textit{t}An^{\bullet+}}$ with **DMB** to the $\mathbf{DAP^{\bullet+}}$ product radical cation is the slowest step of the catalytic cycle. Therefore, oxygen is required for efficient performance to retard unproductive non-geminate back-electron transfer from $\mathbf{PC^{2+}}$ to the long-lived radical cation $\mathbf{\textit{t}An^{\bullet+}}$ by rapid oxidative regeneration of the photocatalyst. The concomitantly formed superoxide and the reduced photocatalyst $\mathbf{PC^{2+}}$ reduce the product radical cation $\mathbf{DAP^{\bullet+}}$ to the Diels-Alder product **DAP** so that $\mathbf{DAP^{\bullet+}}$ does not accumulate. In contrast to $\mathbf{[Cr(dmcbpy)_3]^{3+}}$ and $\mathbf{[Ru(bpz)_3]^{2+}}$ the molecular ruby $\mathbf{[Cr(tpe)_2]^{3+}}$ is exceptionally photo and redoxstable and possesses an ultralong excited state lifetime in the millisecond range. Quantitative conversion is achieved contrary to the photolabile photocatalysts $\mathbf{[Cr(dmcbpy)_3]^{3+}}$ and $\mathbf{[Ru(bpz)_3]^{2+}}$. Furthermore, recycling of $\mathbf{[Cr(tpe)_2]^{3+}}$ is successful without significant loss of activity. This mechanistic and exploratory study of the photoredox properties of a molecular ruby paves the way for an efficient and sustainable utilization of photocatalysts based on Earth-abundant chromium ions, in particular photo- and redoxstable molecular rubies, in oxidative photoredox catalysis.

## DATA AVAILABILITY STATEMENT

The original contributions presented in the study are included in the article/**Supplementary Material**, further inquiries can be directed to the corresponding authors.

## AUTHOR CONTRIBUTIONS

SS conducted the quenching, the catalytic and the UV/Vis/NIR spectroscopic experiments. RN performed and analyzed all laser flash photolysis and many luminescence experiments. KH designed the project and wrote the manuscript. All authors discussed the scientific results and wrote parts of the manuscript.

## FUNDING

This work has been financially supported by the Deutsche Forschungsgemeinschaft (DFG) under grants HE2778/10-2 and INST 247/1018-1.

## ACKNOWLEDGMENTS

We thank Prof. Dr. Christoph Kerzig (Johannes Gutenberg University, Mainz) for the support and usage authorization of the experimental setup of the LFP measurements as well as Alexander Fischer for preparative support, Florian Reichenauer for donation of $[Cr(tpe)_2][BF_4]_3$ and Winald R. Kitzmann for the DFT calculations (Johannes Gutenberg University, Mainz).

## SUPPLEMENTARY MATERIAL

The Supplementary Material for this article can be found online at: https://www.frontiersin.org/articles/10.3389/fchem.2022.887439/full#supplementary-material

## REFERENCE

Aydogan, A., Bangle, R. E., Cadranel, A., Turlington, M. D., Conroy, D. T., Cauët, E., et al. (2021). Accessing Photoredox Transformations with an Iron(III) Photosensitizer and Green Light. *J. Am. Chem. Soc.* 143, 15661–15673. doi:10.1021/jacs.1c06081

Baldo, M. A., Thompson, M. E., and Forrest, S. R. (2000). High-Efficiency Fluorescent Organic Light-Emitting Devices Using a Phosphorescent Sensitizer. *Nature* 403, 750–753. doi:10.1038/35001541

Balzani, V., Bolletta, F., Gandolfi, M. T., and Maestri, M. (1978). Bimolecular Electron Transfer Reactions of the Excited States of Transition Metal Complexes. *Org. Chem. Theor.* 75, 1–64. doi:10.1007/BFb0048835

Baptista, F. A., Krizsan, D., Stitch, M., Sazanovich, I. V., Clark, I. P., Towrie, M., et al. (2021). Adenine Radical Cation Formation by a Ligand-Centered Excited State of an Intercalated Chromium Polypyridyl Complex Leads to Enhanced DNA Photo-Oxidation. *J. Am. Chem. Soc.* 143, 14766–14779. doi:10.1021/jacs.1c06658

Basu, U., Otto, S., Heinze, K., and Gasser, G. (2019). Biological Evaluation of the NIR-Emissive Ruby Analogue $[Cr(ddpd)_2][BF_4]_3$ as a Photodynamic Therapy Photosensitizer. *Eur. J. Inorg. Chem.* 2019, 37–41. doi:10.1002/ejic.201801023

Becker, P. M., Förster, C., Carrella, L. M., Boden, P., Hunger, D., Slageren, J., et al. (2020). Spin Crossover and Long-Lived Excited States in a Reduced Molecular Ruby. *Chem. Eur. J.* 26, 7199–7204. doi:10.1002/chem.202001237

Büldt, L. A., and Wenger, O. S. (2017). Chromium Complexes for Luminescence, Solar Cells, Photoredox Catalysis, Upconversion, and Phototriggered NO Release. *Chem. Sci.* 8, 7359–7367. doi:10.1039/C7SC03372A

Campagna, S., Puntoriero, F., Nastasi, F., Bergamini, G., and Balzani, V. (2007). "Photochemistry and Photophysics of Coordination Compounds: Ruthenium," in *Photochemistry and Photophysics of Coordination Compounds I. Topics in Current Chemistry*. Editors V. Balzani and S. Campagna (Berlin, Heidelberg: Springer), 280, 117–214. doi:10.1007/128_2007_133

Constable, E. C., Housecroft, C. E., Neuburger, M., Schönle, J., and Zampese, J. A. (2014). The Surprising Lability of Bis(2,2′:6′,2′′-Terpyridine)chromium(III) Complexes. *Dalton Trans.* 43, 7227–7235. doi:10.1039/C4DT00200H

Costa, R. D., Ortí, E., Bolink, H. J., Monti, F., Accorsi, G., and Armaroli, N. (2012). Luminescent Ionic Transition-Metal Complexes for Light-Emitting Electrochemical Cells. *Angew. Chem. Int. Ed.* 51, 8178–8211. doi:10.1002/anie.201201471

Crutchley, R. J., and Lever, A. B. P. (1980). Ruthenium(II) Tris(bipyrazyl) Dication - a New Photocatalyst. *J. Am. Chem. Soc.* 102, 7128–7129. doi:10.1021/ja00543a053

Farney, E. P., Chapman, S. J., Swords, W. B., Torelli, M. D., Hamers, R. J., and Yoon, T. P. (2019). Discovery and Elucidation of Counteranion Dependence in Photoredox Catalysis. *J. Am. Chem. Soc.* 141, 6385–6391. doi:10.1021/jacs.9b01885

Förster, C., and Heinze, K. (2020). Photophysics and Photochemistry with Earth-Abundant Metals - Fundamentals and Concepts. *Chem. Soc. Rev.* 49, 1057–1070. doi:10.1039/c9cs00573k

Fulmer, G. R., Miller, A. J. M., Sherden, N. H., Gottlieb, H. E., Nudelman, A., Stoltz, B. M., et al. (2010). NMR Chemical Shifts of Trace Impurities: Common Laboratory Solvents, Organics, and Gases in Deuterated Solvents Relevant to the Organometallic Chemist. *Organometallics* 29, 2176–2179. doi:10.1021/om100106e

Hagfeldt, A., Boschloo, G., Sun, L., Kloo, L., and Pettersson, H. (2010). Dye-sensitized Solar Cells. *Chem. Rev.* 110, 6595–6663. doi:10.1021/cr900356p

Heinemann, F., Karges, J., and Gasser, G. (2017). Critical Overview of the Use of Ru(II) Polypyridyl Complexes as Photosensitizers in One-Photon and Two-Photon Photodynamic Therapy. *Acc. Chem. Res.* 50, 2727–2736. acs.accounts.7b00180. doi:10.1021/acs.accounts.7b00180

Herr, P., Kerzig, C., Larsen, C. B., Häussinger, D., and Wenger, O. S. (2021). Manganese(I) Complexes with Metal-To-Ligand Charge Transfer Luminescence and Photoreactivity. *Nat. Chem.* 13, 956–962. doi:10.1038/s41557-021-00744-9

Higgins, R. F., Fatur, S. M., Damrauer, N. H., Ferreira, E. M., Rappé, A. K., and Shores, M. P. (2018). Detection of an Energy-Transfer Pathway in Cr-Photoredox Catalysis. *ACS Catal.* 8, 9216–9225. doi:10.1021/acscatal.8b03013

Higgins, R. F., Fatur, S. M., Shepard, S. G., Stevenson, S. M., Boston, D. J., Ferreira, E. M., et al. (2016). Uncovering the Roles of Oxygen in Cr(III) Photoredox Catalysis. *J. Am. Chem. Soc.* 138, 5451–5464. doi:10.1021/jacs.6b02723

Hockin, B. M., Li, C., Robertson, N., and Zysman-Colman, E. (2019). Photoredox Catalysts Based on Earth-Abundant Metal Complexes. *Catal. Sci. Technol.* 9, 889–915. doi:10.1039/C8CY02336K

Horibe, T., Ohmura, S., and Ishihara, K. (2019). Structure and Reactivity of Aromatic Radical Cations Generated by $FeCl_3$. *J. Am. Chem. Soc.* 141, 1877–1881. doi:10.1021/jacs.8b12827

Hossain, A., Bhattacharyya, A., and Reiser, O. (2019). Copper's Rapid Ascent in Visible-Light Photoredox Catalysis. *Science* 364, eaav9713. doi:10.1126/science.aav9713

Huber, N., Li, R., Ferguson, C. T. J., Gehrig, D. W., Ramanan, C., Blom, P. W. M., et al. (2020). A PMMA-Based Heterogeneous Photocatalyst for Visible Light-Promoted [4+2] Cycloaddition. *Catal. Sci. Technol.* 10, 2092–2099. doi:10.1039/d0cy00016g

Jamieson, M. A., Serpone, N., Henry, M. S., and Hoffman, M. Z. (1979). Temperature Dependence of the Photoaquation of tris(2,2'-bipyridine) Chromium(III) Ion in Alkaline Solution. *Inorg. Chem.* 18, 214–216. doi:10.1021/ic50191a048

Jiménez, J.-R., Doistau, B., Cruz, C. M., Besnard, C., Cuerva, J. M., Campaña, A. G., et al. (2019). Chiral Molecular Ruby $[Cr(dqp)_2]^{3+}$ with Long-Lived Circularly Polarized Luminescence. *J. Am. Chem. Soc.* 141, 13244–13252. doi:10.1021/jacs.9b06524

Johnston, L. J., and Schepp, N. P. (1995). Laser Flash Photolysis Studies of the Reactivity of Styrene Radical Cations. *Pure Appl. Chem.* 67, 71–78. doi:10.1351/pac199567010071

Johnston, L. J., and Schepp, N. P. (1993). Reactivities of Radical Cations: Characterization of Styrene Radical Cations and Measurements of Their Reactivity toward Nucleophiles. *J. Am. Chem. Soc.* 115, 6564–6571. doi:10.1021/ja00068a013

Kitzmann, W. R., Moll, J., and Heinze, K. (2022). Spin-Flip Luminescence. *Photochem. Photobiol. Sci.* in press. doi:10.1007/s43630-022-00186-3

Leis, W., Argüello Cordero, M. A., Lochbrunner, S., Schubert, H., and Berkefeld, A. (2022). A Photoreactive Iron(II) Complex Luminophore. *J. Am. Chem. Soc.* 144, 1169–1173. doi:10.1021/jacs.1c13083

Leppin, J., Schubert, M., Waldvogel, S. R., and Heinze, K. (2015). Initial Radical Cation Pathway in the $Mo_2Cl_{10}$-Mediated Dehydrogenative Arene Coupling. *Chem. Eur. J.* 21, 4229–4232. doi:10.1002/chem.201406522

Lewis, F. D., and Kojima, M. (1988). Electron-transfer-induced Photoisomerization, Dimerization, and Oxygenation of Trans- and Cis-Anethole. The Role of Monomer and Dimer Cation Radicals. *J. Am. Chem. Soc.* 110, 8664–8670. doi:10.1021/ja00234a014

Li, A., Turro, C., and Kodanko, J. J. (2018). Ru(II) Polypyridyl Complexes Derived from Tetradentate Ancillary Ligands for Effective Photocaging. *Acc. Chem. Res.* 51, 1415–1421. doi:10.1021/acs.accounts.8b00066

Limburg, B., Bouwman, E., and Bonnet, S. (2016). Rate and Stability of Photocatalytic Water Oxidation Using $[Ru(bpy)_3]^{2+}$ as Photosensitizer. *ACS Catal.* 6, 5273–5284. doi:10.1021/acscatal.6b00107

Lin, S., Ischay, M. A., Fry, C. G., and Yoon, T. P. (2011). Radical Cation Diels-Alder Cycloadditions by Visible Light Photocatalysis. *J. Am. Chem. Soc.* 133, 19350–19353. doi:10.1021/ja2093579

Lindh, L., Chábera, P., Rosemann, N. W., Uhlig, J., Wärnmark, K., Yartsev, A., et al. (2020). Photophysics and Photochemistry of Iron Carbene Complexes for Solar Energy Conversion and Photocatalysis. *Catalysts* 10, 315. doi:10.3390/catal10030315

Maestri, M., Bolletta, F., Serpone, N., Moggi, L., and Balzani, V. (1976). Kinetics of Ligand Substitution of tris(2,2'-bipyridine)Chromium(III) in Aqueous Solutions. *Inorg. Chem.* 15, 2048–2051. doi:10.1021/ic50163a007

Magnuson, A., Anderlund, M., Johansson, O., Lindblad, P., Lomoth, R., Polivka, T., et al. (2009). Biomimetic and Microbial Approaches to Solar Fuel Generation. *Acc. Chem. Res.* 42, 1899–1909. doi:10.1021/ar900127h

Marcus, R. A. (1993). Electron Transfer Reactions in Chemistry. Theory and experimentTheory and experiment. *Rev. Mod. Phys.* 65, 599–610. doi:10.1103/RevModPhys.65.599

Mari, C., Pierroz, V., Ferrari, S., and Gasser, G. (2015). Combination of Ru(II) Complexes and Light: New Frontiers in Cancer Therapy. *Chem. Sci.* 6, 2660–2686. doi:10.1039/C4SC03759F

McDaniel, A. M., Tseng, H.-W., Damrauer, N. H., and Shores, M. P. (2010). Synthesis and Solution Phase Characterization of Strongly Photooxidizing Heteroleptic Cr(III) Tris-Dipyridyl Complexes. *Inorg. Chem.* 49, 7981–7991. doi:10.1021/ic1009972

Montalti, M., Credi, A., Prodi, L., and Gandolfi, M. T. (2006). *Handbook of Photochemistry*. 3rd edition. Boca Raton: CRC Press, Taylor&Francis Group LLC.

Murphy, R. S., and Bohne, C. (2000). Use of Styrene Radical Cations as Probes for the Complexation Dynamics of Charged Guests with α- and β-Cyclodextrins. *Photochem. Photobiol.* 71, 35. doi:10.1562/0031-8655(2000)071<0035:uosrca>2.0.co;2

Nakayama, K., Maeta, N., Horiguchi, G., Kamiya, H., and Okada, Y. (2019). Radical Cation Diels-Alder Reactions by $TiO_2$ Photocatalysis. *Org. Lett.* 21, 2246–2250. doi:10.1021/acs.orglett.9b00526

Nozaki, H., Otani, I., Noyori, R., and Kawanisi, M. (1968). Photochemical Reactions of Trans-anethole. *Tetrahedron* 24, 2183–2192. doi:10.1016/0040-4020(68)88120-7

Otto, S., Dorn, M., Förster, C., Bauer, M., Seitz, M., and Heinze, K. (2018a). Understanding and Exploiting Long-Lived Near-Infrared Emission of a Molecular Ruby. *Coord. Chem. Rev.* 359, 102–111. doi:10.1016/j.ccr.2018.01.004

Otto, S., Förster, C., Wang, C., Resch-Genger, U., and Heinze, K. (2018). A Strongly Luminescent Chromium(III) Complex Acid. *Chem. Eur. J.* 24, 12555–12563. doi:10.1002/chem.201802797

Otto, S., Grabolle, M., Förster, C., Kreitner, C., Resch-Genger, U., and Heinze, K. (2015). $[Cr(ddpd)_2]^{3+}$: A Molecular, Water-Soluble, Highly NIR-Emissive Ruby Analogue. *Angew. Chem. Int. Ed.* 54, 11572–11576. doi:10.1002/anie.201504894

Otto, S., Nauth, A. M., Ermilov, E., Scholz, N., Friedrich, A., Resch-Genger, U., et al. (2017). Photo-Chromium: Sensitizer for Visible-Light-Induced Oxidative C–H Bond Functionalization-Electron or Energy Transfer? *ChemPhotoChem* 1, 344–349. doi:10.1002/cptc.201700077

Pal, A. K., Li, C., Hanan, G. S., and Zysman-Colman, E. (2018). Blue-Emissive Cobalt(III) Complexes and Their Use in the Photocatalytic Trifluoromethylation of Polycyclic Aromatic Hydrocarbons. *Angew. Chem. Int. Ed.* 57, 8027–8031. doi:10.1002/anie.201802532

Reichenauer, F., Wang, C., Förster, C., Boden, P., Ugur, N., Báez-Cruz, R., et al. (2021). Strongly Red-Emissive Molecular Ruby $[Cr(bpmp)_2]^{3+}$ Surpasses $[Ru(bpy)_3]^{2+}$. *J. Am. Chem. Soc.* 143, 11843–11855. doi:10.1021/jacs.1c05971

Scarborough, C. C., Sproules, S., Weyhermüller, T., DeBeer, S., and Wieghardt, K. (2011). Electronic and Molecular Structures of the Members of the Electron Transfer Series $[Cr(tbpy)_3]^n$ (N = 3+, 2+, 1+, 0): An X-ray Absorption Spectroscopic and Density Functional Theoretical Study. *Inorg. Chem.* 50, 12446–12462. doi:10.1021/ic201123x

Scattergood, P. A. (2020). Recent Advances in Chromium Coordination Chemistry: Luminescent Materials and Photocatalysis. *Organomet. Chem.* 43, 1–34. doi:10.1039/9781788017077-00001

Schubert, M., Franzmann, P., Wünsche von Leupoldt, A., Koszinowski, K., Heinze, K., and Waldvogel, S. R. (2016). Over-Oxidation as the Key Step in the

Mechanism of the $MoCl_5$ -Mediated Dehydrogenative Coupling of Arenes. *Angew. Chem. Int. Ed.* 55, 1156–1159. doi:10.1002/anie.201508035

Schultz, D. M., Sawicki, J. W., and Yoon, T. P. (2015). An Improved Procedure for the Preparation of $Ru(bpz)_3(PF_6)_2$ via a High-Yielding Synthesis of 2,2'-bipyrazine. *Beilstein J. Org. Chem.* 11, 61–65. doi:10.3762/bjoc.11.9

Singh, P. S., and Evans, D. H. (2006). Study of the Electrochemical Reduction of Dioxygen in Acetonitrile in the Presence of Weak Acids. *J. Phys. Chem. B* 110, 637–644. doi:10.1021/jp055296f

Soupart, A., Alary, F., Heully, J.-L., Elliott, P. I. P., and Dixon, I. M. (2020). Theoretical Study of the Full Photosolvolysis Mechanism of $[Ru(bpy)_3]^{2+}$: Providing a General Mechanistic Roadmap for the Photochemistry of $[Ru(NN)_3]^{2+}$-Type Complexes toward Both Cis and Trans Photoproducts. *Inorg. Chem.* 59, 14679–14695. doi:10.1021/acs.inorgchem.0c01843

Squillacote, M. E., and Liang, F. (2005). Conformational Thermodynamic and Kinetic Parameters of Methyl-Substituted 1,3-Butadienes. *J. Org. Chem.* 70, 6564–6573. doi:10.1021/jo0500277

Stevenson, S. M., Higgins, R. F., Shores, M. P., and Ferreira, E. M. (2017). Chromium Photocatalysis: Accessing Structural Complements to Diels-Alder Adducts with Electron-Deficient Dienophiles. *Chem. Sci.* 8, 654–660. doi:10.1039/c6sc03303b

Stevenson, S. M., Shores, M. P., and Ferreira, E. M. (2015). Photooxidizing Chromium Catalysts for Promoting Radical Cation Cycloadditions. *Angew. Chem. Int. Ed.* 54, 6506–6510. doi:10.1002/anie.201501220

Tanaka, K., Asada, Y., Hoshino, Y., and Honda, K. (2020). Visible-light-induced [4+2] Cycloaddition of Pentafulvenes by Organic Photoredox Catalysis. *Org. Biomol. Chem.* 18, 8074–8078. doi:10.1039/D0OB01151G

Treiling, S., Wang, C., Förster, C., Reichenauer, F., Kalmbach, J., Boden, P., et al. (2019). Luminescence and Light-Driven Energy and Electron Transfer from an Exceptionally Long-Lived Excited State of a Non-Innocent Chromium(III) Complex. *Angew. Chem. Int. Ed.* 58, 18075–18085. doi:10.1002/anie.201909325

Twilton, J., Le, C., Zhang, P., Shaw, M. H., Evans, R. W., and MacMillan, D. W. C. (2017). The Merger of Transition Metal and Photocatalysis. *Nat. Rev. Chem.* 1, 0052. doi:10.1038/s41570-017-0052

Vaidyanathan, V. G., and Nair, B. U. (2004). Nucleobase Oxidation of DNA by (Terpyridyl)chromium( III ) Derivatives. *Eur. J. Inorg. Chem.* 2004, 1840–1846. doi:10.1002/ejic.200300718

Vlcek, A. A., Dodsworth, E. S., Pietro, W. J., and Lever, A. B. P. (1995). Excited State Redox Potentials of Ruthenium Diimine Complexes; Correlations with Ground State Redox Potentials and Ligand Parameters. *Inorg. Chem.* 34, 1906–1913. doi:10.1021/ic00111a043

Wang, C., Kitzmann, W. R., Weigert, F., Förster, C., Wang, X., Heinze, K., et al. (2022). Matrix Effects on Photoluminescence and Oxygen Sensitivity of a Molecular Ruby. *ChemPhotoChem*. in press. doi:10.1002/cptc.202100296

Watson, R. T., Desai, N., Wildsmith, J., Wheeler, J. F., and Kane-Maguire, N. A. P. (1999). Interaction of $Cr(diimine)_3^{3+}$ Complexes with DNA. *Inorg. Chem.* 38, 2683–2687. doi:10.1021/ic980857l

Wenger, O. S. (2018). Photoactive Complexes with Earth-Abundant Metals. *J. Am. Chem. Soc.* 140, 13522–13533. doi:10.1021/jacs.8b08822

Wenger, O. S. (2021). Photoactive Nickel Complexes in Cross-Coupling Catalysis. *Chem. Eur. J.* 27, 2270–2278. doi:10.1002/chem.202003974

Yam, V. W.-W., Chan, A. K.-W., and Hong, E. Y.-H. (2020). Charge-transfer Processes in Metal Complexes Enable Luminescence and Memory Functions. *Nat. Rev. Chem.* 4, 528–541. doi:10.1038/s41570-020-0199-7

Yang, Y., Liu, Q., Zhang, L., Yu, H., and Dang, Z. (2017). Mechanistic Investigation on Oxygen-Mediated Photoredox Diels-Alder Reactions with Chromium Catalysts. *Organometallics* 36, 687–698. doi:10.1021/acs.organomet.6b00886

Yoon, T. P., Ischay, M. A., and Du, J. (2010). Visible Light Photocatalysis as a Greener Approach to Photochemical Synthesis. *Nat. Chem* 2, 527–532. doi:10.1038/nchem.687

**Conflict of Interest:** The authors declare that the research was conducted in the absence of any commercial or financial relationships that could be construed as a potential conflict of interest.

**Publisher's Note:** All claims expressed in this article are solely those of the authors and do not necessarily represent those of their affiliated organizations, or those of the publisher, the editors, and the reviewers. Any product that may be evaluated in this article, or claim that may be made by its manufacturer, is not guaranteed or endorsed by the publisher.

*Copyright © 2022 Sittel, Naumann and Heinze. This is an open-access article distributed under the terms of the Creative Commons Attribution License (CC BY). The use, distribution or reproduction in other forums is permitted, provided the original author(s) and the copyright owner(s) are credited and that the original publication in this journal is cited, in accordance with accepted academic practice. No use, distribution or reproduction is permitted which does not comply with these terms.*